Multipath Detection Metrics and Attenuation Analysis Using a GPS Snapshot Receiver in Harsh Environments

José A. López-Salcedo, Juan Manuel Parro-Jiménez, Gonzalo Seco-Granados
Signal Processing for Communications and Navigation (SPCOMNAV), Universitat Autònoma de Barcelona (UAB)
ETSE, Campus Universitari s/n, 08193 Bellaterra (Barcelona), Spain.
Email: {jose.salcedo, gonzalo.seco}@uab.es

***Abstract*—This paper focuses on the analysis of GPS L1 signals when propagating indoors. Two criteria are proposed with the aim of detecting the presence of multipath, which is one of the major degradations experienced by GPS receivers when operating in indoor environments. The proposed criteria have been evaluated through an exhaustive field test by using a High Sensitivity GNSS software receiver. The results confirm the validity of these criteria and allow a better understanding of the underlying propagation phenomena of GPS signals.**

I. Introduction

In 1996, the US FCC E911 mandate was issued to require location identification for all emergency calls through cellular communication systems. This mandate, followed later by the European E112 recommendation, demands mobile terminals to be able to report their position with an accuracy of 50 meters for 67% of the time, and 150 meters for 95% of the time. This legal requirement has become a primary driver behind the research and development of GNSS receivers, applications and services to be incorporated into future mobile terminals. As an example of the potential market to be faced, note that 1.28 billion terminals are expected to be sold in 2008 according to the consultancy firm Gartner.

This market opportunity, however, involves significant challenges from the technical point of view. Stringent demands are to be fulfilled in terms of very low power consumption, near-instantaneous time-to-first-fix and seamless location in either outdoor or indoor environments. This last requirement is especially challenging when taking into consideration that GNSS have been designed for operation in outdoor environments and not for indoors. In this sense, note that most commercial receivers have their tracking threshold in the range $C/N_0 = 33 - 35$ dBHz. Since the standard outdoor reception conditions provide C/N_0 values on the order of $40 - 45$ dBHz, this leaves a security margin of just 10 dB to accommodate possible power level fluctuations. In the indoor scenario, however, attenuations on the order of 3 dB per meter can easily be found when moving in from an outside wall [1]. Thus, the overall aggregation of blocking obstacles such as walls, doors, ceilings, etc. can introduce signal attenuations on the order of 20 to 70 dB, exceeding by large the available fading margin of commercial GNSS receivers.

This work was supported in part by the Spanish Ministry of Science and Innovation project TEC2008-06305 and the European Space Agency project AO/1-5328/06/NL/GLC.

In order to circumvent this limitation, high-sensitivity (HS) GNSS receivers are being proposed to cope with the severe attenuation and signal degradation of indoor environments [2]. By using HS-GNSS receivers, typical indoor scenarios in the range $C/N_0 = 10 - 25$ dBHz can easily be tackled with, despite of the obstructed sky view. These power levels still allow detection of the received signal by properly extending the overall correlation interval. That is, combining long coherent and noncoherent integrations. However, from the GNSS system perspective, the navigation message cannot be recovered and then external assistance is required to determine the user's position leading to the concept of assisted-GNSS (A-GNSS) [3]. For the case of stand-alone GNSS receivers, connexions must be established to a specific location server where the required assistance information is available.

Based on the concept of A-GNSS, the focus of this paper is to provide an experimental analysis of the indoor propagation conditions undergone by GPS L1 signals. The results of this indoor propagation can be observed in terms of signal attenuation, correlation peak distortion due to multipath components and near-far effects caused by unbalanced power levels between weak and strong visible satellites. In order to assess these degradations, a snapshot mode HS-GNSS software receiver is adopted, which has been developed by the authors in the framework of the ESA project "*Signal Processing Techniques and Demonstrator for Indoor GNSS Positioning*" (DINGPOS).

II. Indoor Signal Characteristics

The signal of GPS-L1 is based on a direct-sequence spread spectrum (DS-SS) scheme where the information bits for satellite m, $b_m(i) = \{-1, +1\}$, are modulated by a pseudo-random spreading code $c_m(k) = \{-1, +1\}$ with $k = 0, 1, \ldots, N_c - 1$ and $N_c = 1023$ chips. Let the discrete-time baseband equivalent of the signal for satellite m be denoted by $s_m(n)$. Then, it follows that

$$s_m(n) = \sum_{i=-\infty}^{\infty} b_m(i) \sum_{k=0}^{N_c N_{sc} N_r - 1} c_m((k)_{N_c}) p(n - iN_{sb} - kN_{sc}) \tag{1}$$

with N_{sc} the number of samples per chip, $N_r = 20$ the GPS-L1 code repetition per bit duration, $(\cdot)_N$ the modulus N operation, N_{sb} the number of samples per bit and $p(n)$ the rectangular shaping pulse with duration N_{sc} samples. In perfect

clear sky conditions where a total of M satellites are in view, the received signal becomes $r(n) = \sum_{m=0}^{M-1} A_m e^{j\omega_m n} s_m(n - \tau_m) + w(n)$ with A_m a complex-valued constant, τ_m the propagation time delay expressed in samples for each satellite, ω_m the residual frequency error due to Doppler and oscillators mismatches and $w(n)$ the additive noise at the receiver with one-sided spectral density $S_w(f) = 2N_0$ W/Hz. Finally, the signal quality for m-th satellite can also be defined in terms of its carrier power to noise spectral density C/N_0 defined as $(C/N_0)_m \doteq \frac{|A_m|^2}{2N_0}$.

A. Signal Attenuation

This is the most important impairment when operating indoors. It is mainly due to blocking obstacles such as building walls, windows and also the roof. Additionally to these building entry losses, extra degradations are often encountered because of the penetration through the building itself [4]. Then, depending on the total signal attenuation, different scenarios can be defined from the resulting C/N_0 values at the receiver end. A typical example is shown in Table I.

TABLE I
TYPICAL C/N_0 RANGE FOR DIFFERENT WORKING SCENARIOS.

	Outdoor	Soft-Indoor	Indoor	Deep-Indoor
C/N_0 (dBHz)	$45-35$	$35-25$	$25-10$	<10

For the experimental results in Section V, different environments have been carefully selected so that they can be representative of the scenarios presented in Table I.

B. Near-Far Effect

Weak and strong satellites can be fairly distinguished as long as their power levels do not differ in more than about 20 dB, assuming GPS-L1 C/A codes. This is a reasonable protection for satellites in outdoor reception but unacceptable for indoor operation where power unbalances on the order of 30 dB can be easily found. The solution to this problem passes through the adoption of near-far mitigation strategies, such as the one based on statistical criteria [5] implemented in the HS-GNSS software receiver used in this paper.

C. Multipath Effect

Surrounding objects in indoor environments may introduce up to R_m reflected rays for the signal coming from m-th satellite. In such a situation, the received signal becomes $r_{\text{multipath}}(n) = r(n) + \sum_{m=0}^{M-1} \sum_{r=0}^{R_m} \alpha_{m,r} e^{j\omega_{m,r} n} s_m(n - \tau'_{m,r})$ with $\alpha_{m,r}$ and $\tau'_{m,r}$ the complex amplitude and delay of each replica, where $\tau'_{m,r} > \tau_m$. At the receiver, the cross-correlation between the incoming signal and the local code becomes the aggregation of multiple correlation peaks, as shown in Fig. 1. This introduces some bias in the position of the first arrival peak and has an impact in the user's position.

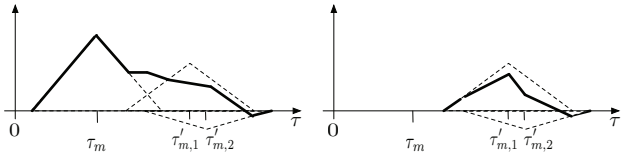

Fig. 1. Correlation peak when multipath is present. (Left) Scenario S1, line-of-sight is present. (Right) Scenario S2, line-of-sight is absent.

III. MULTIPATH DETECTION TECHNIQUE

Multipath has very deleterious effects on the accuracy of GPS and has continuously been the focus of research efforts. Most proposed approaches address the mitigation of multipath effects in the tracking loops. A group of these approaches revolve around identifying the different components that form the total correlation and try to isolate the contribution of the line-of-sight ray (LOS). Experimental results show that this procedure is absolutely impractical in indoor or complex urban scenarios. The reason is that the small multipath delays compared to the correlation width make the identification impossible. Other approaches have exploited the fact that multipath is always delayed wrt the LOS and, allegedly, the left side of the correlation curve should be less affected than the right one. The simplicity of these approaches to mitigate multipath has compensated by a rather limited multipath mitigation capability. In this paper, we intend to exploit the correlation asymmetry to detect multipath degraded scenarios. The detection capability will exceed that achieved for estimation, and moreover multipath detection seems to be much more useful in realistic indoor applications.

A. Slope Asymmetry Metric (SAM)

The proposed multipath detection metric consists on comparing the left and right slopes of the received signal correlation peak. Ideally, both slopes should be equal (but sign reversed) and thus their sum should be theoretically close to zero. The procedure for calculting this metric is the following:

1) The correlation peaks of all available snapshots must be first aligned. To do so, linear piecewise interpolation [5] is performed. The estimated time delay is used for interpolating the original correlation peaks.
2) Normalize the correlation peaks with the square root of an estimate of the C/N_0.
3) For each side of the correlation peak, find the least-squares estimate of the straight line that best fits the three samples next to the maximum of the correlation. The maximum is not included in the set of three samples. The parameters of the line $a\tau + b$ are obtained as $\left[\widehat{a}\ \widehat{b}\right]^T = \mathbf{M}^\sharp \mathbf{y}$ where $\mathbf{M}^\sharp$ is the Moore-Penrose inverse of
$$\mathbf{M} = \begin{bmatrix} -T_s & 0 & T_s \\ 1 & 1 & 1 \end{bmatrix}^T, \tag{2}$$
$\mathbf{y}$ contains the three side samples of the interpolated correlation, and T_s is the time spacing between them.
4) The slope asymmetry metric is defined as
$$\text{SAM} \doteq \widehat{a}_l + \widehat{a}_r\,, \tag{3}$$
where $\widehat{a}_l$ and $\widehat{a}_r$ are the estimated slopes of the left and right sides of the correlation peak, respectively.

The mean and the variance of the SAM can be used as indicators of the presence of multipath. In particular, a mean different to zero would reveal that on average both slopes are different, and one would expect this situation to happen in a static multipath scenario. If multipath conditions are changing during the period spanned by the processed snapshots, the average difference (μ_{SAM}) between the slopes on both sides

will tend to vanish even though the slopes are markedly different during a portion of the snapshots.

Since the correlation peak has been normalized with the square root of C/N_0, the variance of the SAM (σ_{SAM}) should ideally be independent of the C/N_0 and hence the same for all satellites. If σ_{SAM} presents larger values for some satellites, this means that the slopes of the correlation have a variability larger than that caused by noise. The increased variability is an indicator of multipath because if multipath is present, the changing constructive/destructive combination of correlation contributions from different paths distorts the total correlation peak, increasing the difference between both slopes.

The capability of this metric to detect the presence of multipath will be confirmed by the experimental results. However, the metric is not able to distinguish between the two situations sketched in Fig. 1. The left subplot corresponds to an scenario (S1) where the LOS component is received together with several multipath components. Because of their relative additional delays, their effect is more evident in the right slope of the correlation peak of the LOS component than on the left one. The right subplot represents a situation (S2) where the multipath adds together without the presence of the LOS ray.

B. Slope Coherence Time (SCT)

The SCT is proposed as a metric to assess where the scenario is closer to S1 or S2, that is to say, to quantify the extent to which the LOS is present. Note that S1 and S2 are extreme cases and, in practice, one usually finds intermediate situations. This metric is intended to measure the closeness to the extreme cases, once significant multipath has been detected using the SAM. If the SAM is obtained for several snapshots, indexed by l, the time correlation of the SAM at lag k can be estimated as $R_{\mathrm{SAM}}(k) = \sum_l \mathrm{SAM}(l+k)\mathrm{SAM}(l)$. The SCT is defined as the width (e.g. at the half-height level) of $R_{\mathrm{SAM}}(k)$. Note that the same idea could also be applied with $\widehat{a}_r$.

In the absence of multipath, the slopes are only affected by noise, which is independent between snapshots. Therefore, $R_{\mathrm{SAM}}(k)$ tends to be zero for all lags except for $k = 0$. This means that the SCT tends to be null. In case S1, the right slope changes as a function of the relative phases between the LOS and multipath components. These phases vary according to the constellation geometry and the movement of the reflectors. In general, this variation is slow, which results in a wide $R_{\mathrm{SAM}}(k)$ and hence in a large SCT (on the order of tens of seconds). In case S2, the slopes are determined by the addition of multipath components only. This leads to potentially faster slope changes than in S1. One expects to find oscillations in the $R_{\mathrm{SAM}}(k)$, which are determined only by changes in the proximity of the receiver. As a consequence, the expected value of SCT is smaller than in S1 but larger than in a multipath-free scenario.

IV. Experimental Set-Up

A. Working Conditions

The evaluation of the two proposed criteria for multipath detection has been carried out by using signals gathered in different scenarios. Two groups of measurements have been obtained. The first one corresponds to a typical residential building where raw signals have been captured both outdoors and indoors, as shown in the measurement positions "p1", "p2" and "p3" of Fig. 2.

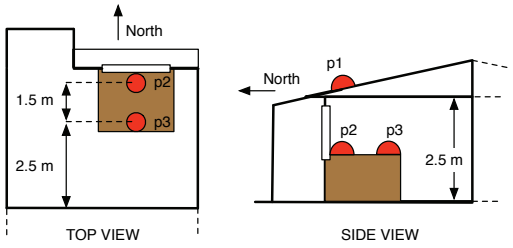

Fig. 2. Sketch of the top floor of the residential building where raw signals were acquired.

The second group of measurements were acquired from a corridor in-between buildings as shown in Fig. 3. The height of these buildings is about 15 meters and their separation, at the point where measurements were taken is 20 meters.

Fig. 3. Location (red circle) where the canyon raw signals were taken.

B. Sky Plots for the Considered Scenarios

The sky plot for the two groups of measurements is shown in Fig. 4. It represents the polar plot of each visible satellite, an information that will often help us to understand the degradations effects that the received signals may have experienced.

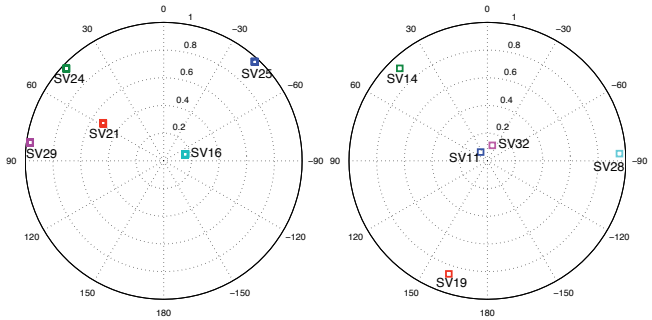

Fig. 4. (Left) Polar plot of visible satellites at "p1" in Fig. 2 on Jan 17, 2009, 09:01:46 GPS time. (Right) Polar plot of visible satellites at the canyon measurement position in Fig. 3 on Dec 22, 2008, 16:21:07 GPS time.

C. Test Equipment

The test equipment consists of a GPS-L1 patch antenna connected to a Nordnav R-25 front-end. The front-end implements downconversion to an intermediate frequency of 4.1304 MHz, bandpass filtering of 2 MHz and analog-to-digital conversion with sampling frequency 16.3676 MHz at 2 bits per sample. The discrete-time samples are stored in disk for offline processing with a HS-GNSS receiver [2], which operates in snapshot mode. To reduce the overall computational burden, the HS-GNSS receiver decimates the input signal down to a sampling frequency of 4.0919 MHz.

V. Analysis of GPS L1 Raw Signals

A. Residential Outdoor Scenario

The samples for this scenario were taken by placing the antenna on the roof of a residential building, as shown in position "p1" of Fig. 2, and setting the HS-GNSS receiver with a total integration time of 80 ms. The building was surrounded by other constructions with similar height and no significant blocking obstacles were present. As a result, perfect clear sky conditions can be assumed. The only possible reduction of the sky view came from the roof inclination. This effect can be observed in the left hand side plot of Fig. 4, where visible satellites are mainly found in the upper half of the polar plot.

The results for this scenario are summarized in Fig. 5, where the estimated C/N_0, the SAM and the shape of the interpolated correlation peaks of each satellite are illustrated. Regarding the C/N_0 values, they can be seen to lie within the typical range of 35-45 dBHz for outdoor reception. Accordingly, the correlation peaks show a sharp and clear shape, which confirms the absence of any relevant propagation impairment. This is consistent with the reduced values of the SAM metric, which indicates that the symmetry of the left and right slopes is being preserved. For all these reasons, the results for this scenario will be considered to be the baseline for the rest of test cases to be analyzed.

B. Residential Near-Window Scenario

The samples for this scenario were taken by placing the antenna close to the window, as shown in position "p2" of Fig. 2, and setting the HS-GNSS with a total integration time of 1 second per snapshot. In this scenario we would be expecting a strong line-of-sight (the signal coming through the window) plus reflections coming from surrounding close indoor objects. According to Fig. 6, the strongest signal is here the one corresponding to SV25. This is consistent with the sky plot of Fig. 4, since SV25 is more likely the satellite with line-of-sight propagation at the measurement position "p2". All the rest of signals have to penetrate through solid blocking obstacles, and thus, their C/N_0 values are significantly attenuated. This is the case of SV21, SV24 and SV29, which are attenuated by the prominent walls on the left hand side of the building. The remaining visible satellite, SV16, is placed over roof of the building. Thus, its signal is attenuated by the roof materials, consisting on reinforced concrete and asphalt membranes. The losses for SV16 are around 25dB in C/N_0.

The results for the SAM are shown in Fig. 7. The top plot shows the evolution of this metric with time (left) and its dispersion for each of the visible satellites (right). From the SAM values, it becomes clear that SV25 has the most symmetric correlation peaks. For the rest of satellites, the dispersion of SAM values confirms the presence of multipath, and the reduced SCT suggests fast slope changes, which are typical of indoor reflecting signals.

C. Canyon Scenario

The samples for this scenario were taken at the measurement position indicated in Fig. 3, and setting the HS-GNSS total integration time to 300ms per snapshot. The aim of this test is to emulate the urban canyon propagation characterized by reduced sky visibility, but also strong multipath components from reflecting signals in the surrounding buildings.

Signals from SV11 and SV32 are the strongest ones, coming from elevation angles close to 90 and no blocking obstacles in-between. Their received C/N_0 levels are on the order of 38-44 dBHz, typical for clear sky outdoor conditions. The rest of signals are degraded by the presence of buildings and affected by reflections. This is especially true for the case of signals from SV28 and SV29, which arrive with a very low elevation angle from the East and South directions, respectively. In these circumstances, signals from SV28 and SV29 are likely to enter the canyon structure and reflect from side to side of the canyon. Such a multipath situation is the one described by the large variations of the SAM in Fig. 9, and confirmed when observing the SCT, which amounts 50 snapshots (15 seconds) for SV32 and 75 snapshots (22.5 seconds) for SV14.

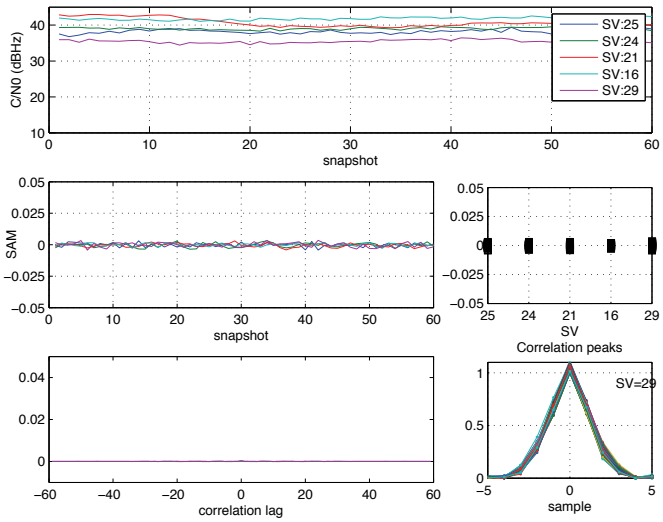

Fig. 5. (Top) C/N0 for satellites at position "p1". (Center) SAM. (Bottom Left) Correlation of SAM samples. (Bottom Right) Correlation peaks for the satellite with worst C/N0 value.

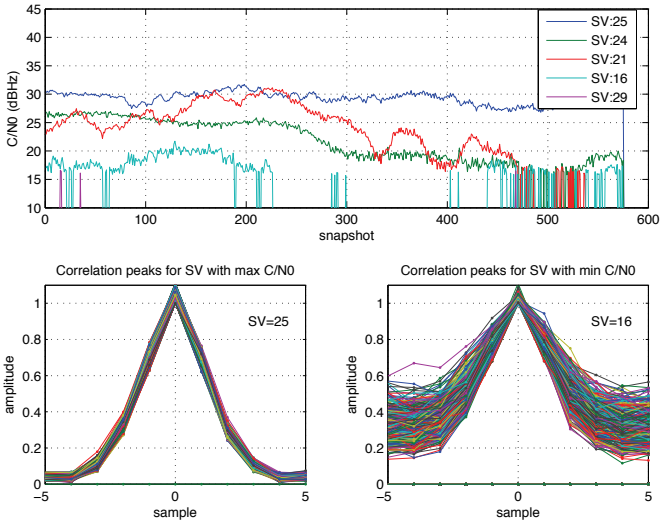

Fig. 6. (Top) Estimated C/N0 values for the visible satellites at position "p2". (Bottom) Correlation peaks for the satellites with maximum (left) and minimum (right) C/N0 values at that position.

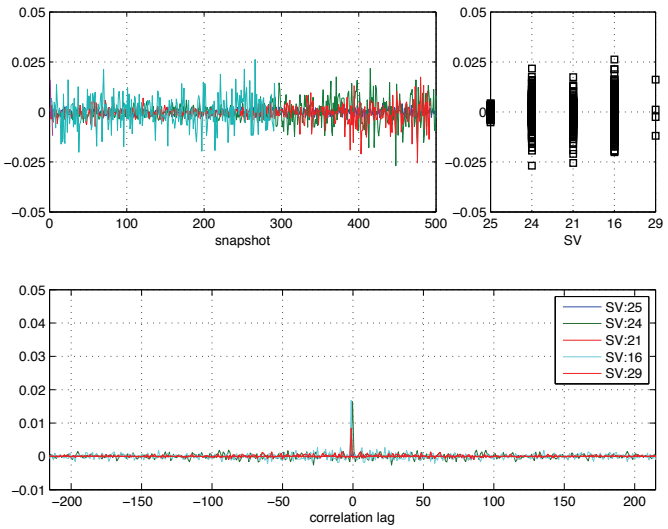

Fig. 7. (Top) SAM at position "p2". (Bottom) SAM correlation.

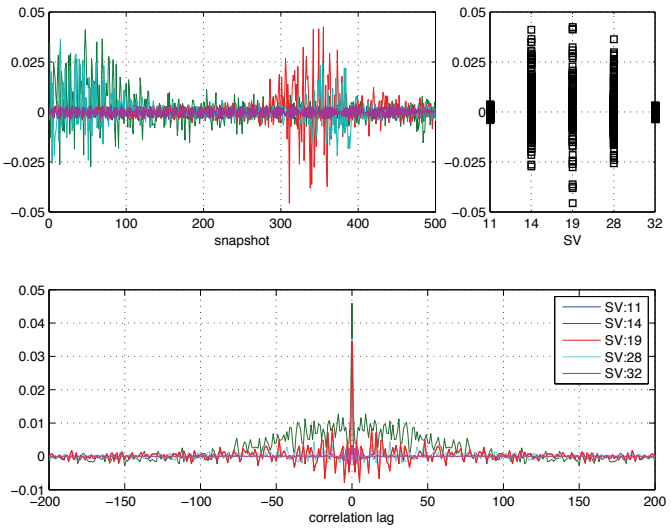

Fig. 9. (Top) SAM at the canyon scenario. (Bottom) SAM correlation.

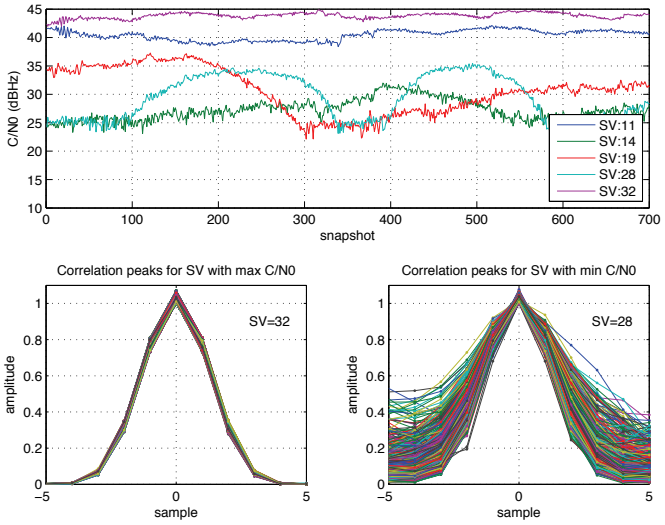

Fig. 8. (Top) Estimated C/N0 values for the visible satellites at the canyon scenario. (Bottom) Correlation peaks for the satellites with maximum (left) and minimum (right) C/N0 values at that scenario.

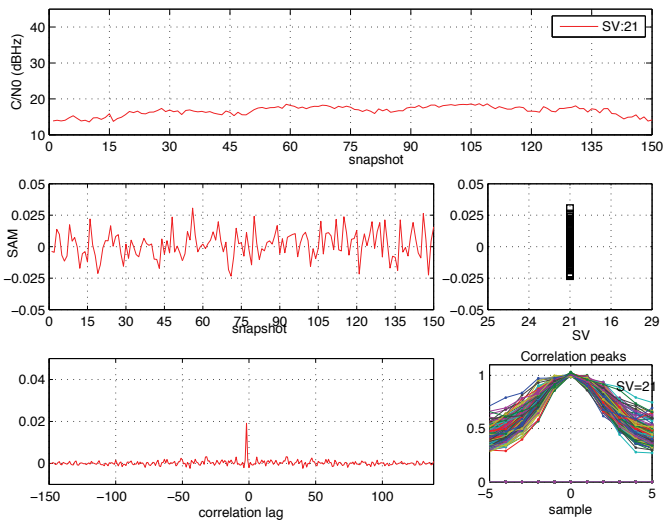

Fig. 10. (Top) Estimated C/N0 values for visible satellites at position "p3". (Center) SAM. (Bottom Left) Correlation of SAM samples. (Bottom Right) Correlation peaks for SV21.

D. Residential Indoor Scenario

In this scenario, the antenna is placed at the measurement position "p3" in Fig. 2. The result is a non-line-of-sight (NLOS) propagation environment with all satellites being obstructed with walls. Signals captured indoors are also expected to be degraded due to multiple reflections with furniture and other close obstacles, so detecting these signals in practice becomes a rather difficult task. The results shown in Fig. 10 confirm this intuition. For a total integration time of 3 seconds, just SV21 is visible, with its C/N_0 lying from 12-19 dBHz during the observation interval. The SAM in the central plot of Fig. 10 exhibits a significant jitter, comparable to the one observed for the canyon scenario in Fig. 9. However, the SCT is much smaller in the indoor case due to the fast variations of signal reflections arriving at the receive antenna.

VI. Conclusions

This paper has presented a set of experimental results for illustrating the propagation effects of GPS L1 signals in different scenarios, from outdoors to indoors. Tests have been carried out by using a HS-GNSS and a NordNav front-end for the acquisition of samples. From the analysis of the resulting data, two metrics have been proposed for helping in the detection of multipath impairments, which in practice, cause a significant bias when solving the user's position.

References

[1] B. B. Peterson, D. Bruckner, and S. Heye, "Measuring GPS Signals Indoors," in *Proc. Institute of Navigation (ION),*, November 1997.

[2] J. A. López-Salcedo, Y. Capelle, M. Toledo, G. Seco, J. L. Vicario, D. Kubrak, M. Monnerat, A. Mark, and D. Jiménez-Banos, "DINGPOS: A Hybrid Indoor Navigation Platform for GPS and GALILEO," in *Proc. 21st ION GNSS*, 2008, pp. 1780–1791.

[3] M. Monnerat, "AGNSS Standarization," *Inside GNSS*, Jul.-Aug. 2008.

[4] F. Perez-Fontan, V. Hovinen, E. Kubista, R. Wack, M. Schonhuber, and R. Prieto-Cerdeira, "Characterization of the Satellite-to-Indoor Channel at S-band," in *Proc. EuCAP*, Nov. 2007, pp. 1–7.

[5] G. López-Risueno and G. Seco, "C/N0 Estimation and Near-Far Mitigation for GNSS Indoor Receivers," in *Proc. IEEE Veh. Technol. Conf. (VTC)*, vol. 4, June 2005, pp. 2624–2628.